CHAPTER 7

Microkinetic Analysis of Catalytic Reactions

7.1 | Introduction

A catalytic reaction consists of many elementary steps that comprise an overall mechanistic path of a chemical transformation. Although rigorous reaction mechanisms are known for simple chemical reactions, many catalytic reactions have been adequately described by including only the kinetically significant elementary steps. This approach was used in Chapter 5 to simplify complex heterogeneous catalytic reaction sequences to kinetically relevant surface reactions. The next step in furthering our understanding of catalytic reactions is to consolidate the available experimental data and theoretical principles that pertain to elementary steps in order to arrive at quantitative models. This is the role of microkinetic analysis, which is defined as an examination of catalytic reactions in terms of elementary steps and their relation with each other during a catalytic cycle (J. A. Dumesic, D. F. Rudd, L. M. Aparicio, J. E. Rekoske, and A. A. Trevino, *The Microkinetics of Heterogeneous Catalysis,* American Chemical Society, Washington, D.C., 1993, p. 1). In this chapter, three catalytic reactions will be examined in detail to illustrate the concept of microkinetic analysis and its relevance to chemical reaction engineering. The first example is asymmetric hydrogenation of an olefin catalyzed by a soluble organometallic catalyst. The second and third examples are ammonia synthesis and olefin hydrogenation, respectively, on heterogeneous transition metal catalysts.

7.2 | Asymmetric Hydrogenation of Prochiral Olefins

The use of soluble rhodium catalysts containing chiral ligands to obtain high stereoselectivity in the asymmetric hydrogenation of prochiral olefins represents one of the most important achievements in catalytic selectivity, rivaling the stereoselectivity of enzyme catalysts [J. Halpern, *Science,* **217** (1982) 401]. Many chiral ligands

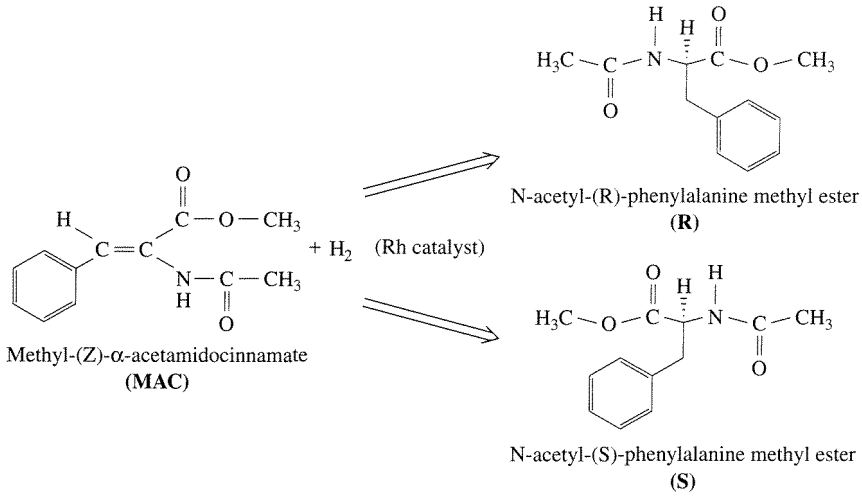

Figure 7.2.1 |
Hydrogenation of **MAC** catalyzed by a homogeneous Rh catalyst to give **R** and **S** enantiomers of N-acetylphenylalanine methyl ester.

have been used to create this class of new asymmetric hydrogenation catalysts. In addition, stereoselectivity has been observed with a variety of olefins during hydrogenation reactions in the presence of these chiral catalysts, demonstrating the general utility of the materials. As an example of microkinetic analysis, the asymmetric hydrogenation of methyl-(Z)-α-acetamidocinnamate, or **MAC,** to give the enantiomers (**R** and **S**) of N-acetylphenylalanine methyl ester will be discussed in detail. The overall reaction is illustrated in Figure 7.2.1.

C. R. Landis and J. Halpern found that cationic rhodium, Rh(I), with the chiral ligand R,R-1,2-bis[(phenyl-o-anisol)phosphino]ethane, or DIPAMP (see Figure 7.2.2), was very selective as a catalyst for the production of the **S** enantiomer of

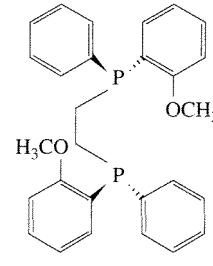

R,R-DIPAMP
R,R-1,2-bis[(phenyl-o-anisol)phosphino]ethane

Figure 7.2.2 |
Chiral ligand for enantioselective rhodium catalyst

N-acetylphenylalanine methyl ester during **MAC** hydrogenation in methanol solvent [C. R. Landis and J. Halpern, *J. Am. Chem. Soc.*, **109** (1987) 1746]. The DIPAMP coordinates to the rhodium through the phosphorus atoms and leaves plenty of space around the Rh cation for other molecules to bind and react. The unique feature of this system is that the chirality of the DIPAMP ligand induces the high stereoselectivity of the product molecules. An analogous nonchiral ligand on the Rh cation produces a catalyst that is not enantioselective.

To understand the origin of enantioselectivity in this system, the kinetics of the relevant elementary steps occurring during hydrogenation had to be determined. The catalytic cycle can be summarized as: (a) reversible binding of the olefin (**MAC**) to the Rh catalyst, (b) irreversible addition of dihydrogen to the Rh-olefin complex, (c) reaction of hydrogen with the bound olefin, and (d) elimination of the product into the solution to regenerate the original catalyst. Landis and Halpern have measured the kinetics of step (a) as well as the overall reactivity of the adsorbed olefin with dihydrogen [C. R. Landis and J. Halpern, *J. Am. Chem. Soc.*, **109** (1987) 1746]. Figure 7.2.3 shows two coupled catalytic cycles that occur in parallel for the production of **R** and **S** enantiomers from **MAC** in the presence of a common rhodium catalyst, denoted as *. Since the catalyst has a chiral ligand, **MAC** can add to the catalyst in two different forms, one that leads to the **R** product, called $\mathbf{MAC}^{*\mathbf{R}}$, and one that leads to the **S** product, called $\mathbf{MAC}^{*\mathbf{S}}$. The superscripts refer to the catalytic cycles that produce the two enantiomers.

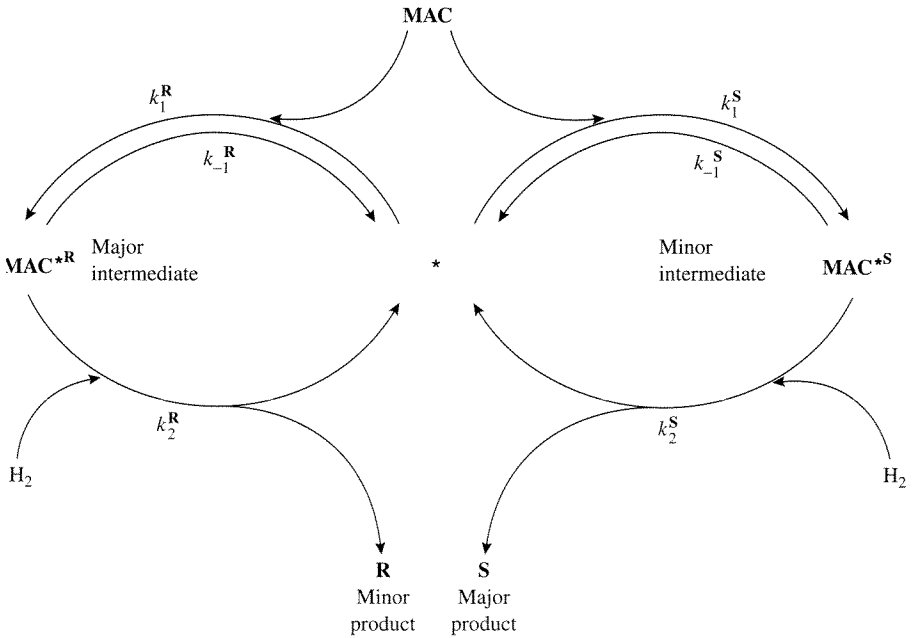

Figure 7.2.3 |
Scheme of the coupled catalytic cycles for the asymmetric hydrogenation of **MAC.**

Expressions for relative concentrations of the intermediates and products are developed from concepts discussed in earlier chapters, namely, the use of a total catalytic site balance and the application of the steady-state approximation. The total amount of rhodium catalyst in the reactor is considered constant, $[*]_0$, so that the site balance becomes:

$$[*]_0 = [\mathbf{MAC}^{*\mathbf{R}}] + [\mathbf{MAC}^{*\mathbf{S}}] + [*] \tag{7.2.1}$$

The steady-state approximation indicates that the concentrations of reactive intermediates remain constant with time. In other words, the net rate of **MAC** binding to the catalyst to form an intermediate must be the same as the rate of hydrogenation (or disappearance) of the intermediate. The steady-state approximation for the coupled catalytic cycles is expressed mathematically as:

$$\frac{d[\mathbf{MAC}^{*\mathbf{R}}]}{dt} = 0 = r_1^{\mathbf{R}} - r_{-1}^{\mathbf{R}} - r_2^{\mathbf{R}} \tag{7.2.2}$$

$$\frac{d[\mathbf{MAC}^{*\mathbf{S}}]}{dt} = 0 = r_1^{\mathbf{S}} - r_{-1}^{\mathbf{S}} - r_2^{\mathbf{S}} \tag{7.2.3}$$

or in terms of the rate expressions as:

$$0 = k_1^{\mathbf{R}}[\mathbf{MAC}][*] - k_{-1}^{\mathbf{R}}[\mathbf{MAC}^{*\mathbf{R}}] - k_2^{\mathbf{R}}[\mathbf{MAC}^{*\mathbf{R}}][H_2] \tag{7.2.4}$$

$$0 = k_1^{\mathbf{S}}[\mathbf{MAC}][*] - k_{-1}^{\mathbf{S}}[\mathbf{MAC}^{*\mathbf{S}}] - k_2^{\mathbf{S}}[\mathbf{MAC}^{*\mathbf{S}}][H_2] \tag{7.2.5}$$

Rearranging Equations (7.2.4 and 7.2.5) gives the concentrations of reactive intermediates:

$$[\mathbf{MAC}^{*\mathbf{R}}] = \frac{k_1^{\mathbf{R}}[\mathbf{MAC}][*]}{k_{-1}^{\mathbf{R}} + k_2^{\mathbf{R}}[H_2]} \tag{7.2.6}$$

$$[\mathbf{MAC}^{*\mathbf{S}}] = \frac{k_1^{\mathbf{S}}[\mathbf{MAC}][*]}{k_{-1}^{\mathbf{S}} + k_2^{\mathbf{S}}[H_2]} \tag{7.2.7}$$

that can be used to derive an equation for their relative concentration:

$$\frac{[\mathbf{MAC}^{*\mathbf{S}}]}{[\mathbf{MAC}^{*\mathbf{R}}]} = \left(\frac{k_1^{\mathbf{S}}}{k_1^{\mathbf{R}}}\right)\frac{k_{-1}^{\mathbf{R}} + k_2^{\mathbf{R}}[H_2]}{k_{-1}^{\mathbf{S}} + k_2^{\mathbf{S}}[H_2]} \tag{7.2.8}$$

The ratio of concentrations of the products **R** and **S** can be derived in a similar fashion:

$$r_{\mathbf{R}} = r_1^{\mathbf{R}} - r_{-1}^{\mathbf{R}} = r_2^{\mathbf{R}} \tag{7.2.9}$$

$$r_{\mathbf{S}} = r_1^{\mathbf{S}} - r_{-1}^{\mathbf{S}} = r_2^{\mathbf{S}} \tag{7.2.10}$$

$$\frac{[\mathbf{S}]}{[\mathbf{R}]} = \frac{r_{\mathbf{S}}}{r_{\mathbf{R}}} = \frac{r_2^{\mathbf{S}}}{r_2^{\mathbf{R}}} = \frac{k_2^{\mathbf{S}}[\mathbf{MAC}^{*\mathbf{S}}][H_2]}{k_2^{\mathbf{R}}[\mathbf{MAC}^{*\mathbf{R}}][H_2]} = \left(\frac{k_2^{\mathbf{S}}}{k_2^{\mathbf{R}}}\right)\frac{[\mathbf{MAC}^{*\mathbf{S}}]}{[\mathbf{MAC}^{*\mathbf{R}}]} \tag{7.2.11}$$

Table 7.2.1 | Kinetic parameters for the asymmetric hydrogenation of MAC catalyzed by Rh(R,R-DIPAMP) at 298 K.

Parameter	R Cycle	S Cycle
k_1 (L mmol^{-1} s^{-1})	5.3	11
k_{-1} (s^{-1})	0.15	3.2
K_1 (L mmol^{-1})	35	3.3
k_2 (L mmol^{-1} s^{-1})	1.1×10^{-3}	0.63

Source: C. R. Landis and J. Halpern, *J. Am. Chem. Soc.*, **109** (1987) 1746.

The relative concentration of reactive intermediates given in Equation (7.2.8) is then substituted into Equation (7.2.11) to give the ratio of final products:

$$\frac{[\mathbf{S}]}{[\mathbf{R}]} = \left(\frac{k_1^{\mathbf{S}} k_2^{\mathbf{S}}}{k_1^{\mathbf{R}} k_2^{\mathbf{R}}}\right) \frac{k_{-1}^{\mathbf{R}} + k_2^{\mathbf{R}}[\mathrm{H_2}]}{k_{-1}^{\mathbf{S}} + k_2^{\mathbf{S}}[\mathrm{H_2}]} \tag{7.2.12}$$

Notice that the relative concentrations of the intermediates and products depend only on temperature (through the individual rate constants) and the pressure of dihydrogen.

At sufficiently low dihydrogen pressures, the reversible binding of **MAC** to the catalyst is essentially equilibrated because:

$$k_{-1}^{\mathbf{R}} >> k_2^{\mathbf{R}}[\mathrm{H_2}] \tag{7.2.13}$$

and

$$k_{-1}^{\mathbf{S}} >> k_2^{\mathbf{S}}[\mathrm{H_2}] \tag{7.2.14}$$

In other words, the rate-determining step for the reaction at low dihydrogen pressures is the hydrogenation of bound olefin. Simplification of Equations (7.2.8) and (7.2.12) by assuming low dihydrogen pressure gives the following expressions for the relative concentrations of intermediates and products:

$$\frac{[\mathbf{MAC}\ ^{*\mathbf{S}}]}{[\mathbf{MAC}\ ^{*\mathbf{R}}]} = \left(\frac{k_1^{\mathbf{S}}}{k_1^{\mathbf{R}}}\right) \frac{k_{-1}^{\mathbf{R}}}{k_{-1}^{\mathbf{S}}} = \frac{K_1^{\mathbf{S}}}{K_1^{\mathbf{R}}} \tag{7.2.15}$$

$$\frac{[\mathbf{S}]}{[\mathbf{R}]} = \left(\frac{k_1^{\mathbf{S}} k_2^{\mathbf{S}}}{k_1^{\mathbf{R}} k_2^{\mathbf{R}}}\right) \frac{k_{-1}^{\mathbf{R}}}{k_{-1}^{\mathbf{S}}} = \frac{K_1^{\mathbf{S}}}{K_1^{\mathbf{R}}} \frac{k_2^{\mathbf{S}}}{k_2^{\mathbf{R}}} \tag{7.2.16}$$

Landis and Halpern have measured the relevant rate constants for this reaction system and they are summarized in Table 7.2.1 [C. R. Landis and J. Halpern, *J. Am. Chem. Soc.*, **109** (1987) 1746].

The values of the measured constants indicate that the **S** enantiomer is greatly favored over the **R** enantiomer at 298 K:

$$\frac{[\mathbf{S}]}{[\mathbf{R}]} = \frac{K_1^{\mathbf{S}} k_2^{\mathbf{S}}}{K_1^{\mathbf{R}} k_2^{\mathbf{R}}} = \frac{3.3}{35} \cdot \frac{0.63}{1.1 \times 10^{-3}} = 54 \tag{7.2.17}$$

This result is rather surprising since the reactive intermediate that leads to the **S** enantiomer is in the minority. Equation (7.2.15) illustrates the magnitude of this difference:

$$\frac{[\mathbf{MAC}\ ^{*\mathbf{S}}]}{[\mathbf{MAC}\ ^{*\mathbf{R}}]} = \frac{K_1^{\mathbf{S}}}{K_1^{\mathbf{R}}} = 0.094 \tag{7.2.18}$$

The reason that the *minor* reactive intermediate leads to the *major* product is due to the large rate constant for hydrogenation (k_2) associated with the **S** cycle compared to the **R** cycle. Clearly, the conventional "lock and key" analogy for the origin of enantioselectivity does not apply for this case since the selectivity is determined by kinetics of hydrogenation instead of thermodynamics of olefin binding.

A microkinetic analysis of this system also adequately explains the dependence of enantioselectivity on dihydrogen pressure. At sufficiently high pressures of dihydrogen,

$$k_{-1}^{\mathbf{R}} << k_2^{\mathbf{R}}[\mathrm{H_2}] \tag{7.2.19}$$

and

$$k_{-1}^{\mathbf{S}} << k_2^{\mathbf{S}}[\mathrm{H_2}] \tag{7.2.20}$$

Since the binding of olefin is not quasi-equilibrated at high pressure, the subsequent hydrogenation step cannot be considered as rate-determining. The relative concentrations of reactive intermediates and products are now given as:

$$\frac{[\mathbf{MAC}\ ^{*\mathbf{S}}]}{[\mathbf{MAC}\ ^{*\mathbf{R}}]} = \left(\frac{k_1^{\mathbf{S}}}{k_1^{\mathbf{R}}}\right)\frac{k_2^{\mathbf{R}}}{k_2^{\mathbf{S}}} = \left(\frac{11}{5.3}\right)\frac{1.1 \times 10^{-3}}{0.63} = 3.6 \times 10^{-3} \tag{7.2.21}$$

and

$$\frac{[\mathbf{S}]}{[\mathbf{R}]} = \left(\frac{k_1^{\mathbf{S}}}{k_1^{\mathbf{R}}}\right) = \left(\frac{11}{5.3}\right) = 2.1 \tag{7.2.22}$$

The effect of dihydrogen is to lower the enantioselectivity to the **S** product from [**S**]/[**R**] = 54 at low pressures to [**S**]/[**R**] = 2.1 at high pressures. The reason for the drop in selectivity is again a kinetic one. The *kinetic coupling* of the olefin binding and hydrogenation steps becomes important at high dihydrogen pressure [M. Boudart and G. Djega-Mariadassou, *Catal. Lett.*, **29** (1994) 7]. In other words, the rapid hydrogenation of the reactive intermediate prevents quasi-equilibration of the olefin binding step. The relative concentration of the *minor* intermediate $\mathbf{MAC}^{*\mathbf{S}}$ (that leads to the *major* product **S**) decreases significantly with increasing dihydrogen pressure since $k_2^{\mathbf{S}} >> k_2^{\mathbf{R}}$. In this example, the kinetic coupling on the **S** cycle is much stronger than that on the **R** cycle, and that leads to an overall reduction in selectivity with increasing dihydrogen pressure.

It should be pointed out that selectivity does not depend on dihydrogen in the limit of very high or very low pressure. For intermediate dihydrogen pressures, Equations (7.2.8) and (7.2.12)—that depend on dihydrogen—should be used to calculate selectivity. The microkinetic methodology satisfactorily explains the surprising

inverse relationship between intermediate and product selectivity and the unusual effect of dihydrogen pressure on product selectivity observed during asymmetric hydrogenation of prochiral olefins with a chiral catalyst.

7.3 | Ammonia Synthesis on Transition Metal Catalysts

The ammonia synthesis reaction is one of the most widely studied reactions and it has been discussed previously in this text. (See Example 1.1.1, Table 5.2.1, and Section 5.3.) In this section, results from the microkinetic analysis of ammonia synthesis over transition metal catalysts containing either iron or ruthenium will be presented.

A conventional ammonia synthesis catalyst, based on iron promoted with Al_2O_3 and K_2O, operates at high temperatures and pressures in the range of 673–973 K and 150–300 bars to achieve acceptable production rates. Metallic iron is the active catalytic component while Al_2O_3 and K_2O act as structural and chemical promoters, respectively. The goal of microkinetic analysis in this case is to study the conditions under which data collected on single crystals in ultrahigh vacuum or on model powder catalysts at ambient pressures can be extrapolated to describe the performance of a working catalyst under industrial conditions of temperature and pressure. Unfortunately, the kinetic parameters of all possible elementary steps are not known for most heterogeneous catalytic reactions. Thus, a strategy adopted by Dumesic et al. involves construction of a serviceable reaction path that captures the essential surface chemistry, and estimation of relevant parameters for kinetically significant elementary steps (J. A. Dumesic, D. F. Rudd, L. M. Aparicio, J. E. Rekoske, and A. A. Trevino, *The Microkinetics of Heterogeneous Catalysis,* American Chemical Society, Washington, D.C., 1993, p. 145).

In the case of ammonia synthesis on transition metal catalysts, a variety of reasonable paths with various levels of complexity can be proposed. For the sake of clarity, only one such path will be presented here. Stolze and Norskov successfully interpreted the high-pressure kinetics of ammonia synthesis based on a microscopic model established from fundamental surface science studies [P. Stolze and J. K. Norskov, *Phys. Rev. Lett.,* **55** (1985) 2502; P. Stolze and J. K. Norskov, *J. Catal.,* **110** (1988) 1]. Dumesic et al. re-analyzed that sequence of elementary steps, which is presented in Table 7.3.1, for ammonia synthesis over iron catalysts [J. A. Dumesic and A. A. Trevino, *J. Catal.,* **116** (1989) 119]. The rate constants for adsorption and desorption steps were estimated from results obtained on iron single crystal surfaces at ultrahigh vacuum conditions. The surface hydrogenation rates were estimated from the relative stabilities of surface NH_X species. In the following microkinetic analysis, an industrial plug flow reactor was modeled as a series of 10,000 mixing cells (see Example 3.4.3) in which the steady-state rate equations, the catalyst site balance, and the material balances for gaseous species were solved simultaneously. Thus, no assumptions with respect to a possible rate-determining step and a most abundant reaction intermediate were needed to complete the model.

The conditions chosen for the microkinetic analysis correspond to an industrial reactor with 2.5 cm^3 of catalyst operating at 107 bar with a stoichiometric feed of

Table 7.3.1 | A proposed mechanism of ammonia synthesis over iron catalysts.[a]

Number	Forward rate	Elementary step	Reverse rate
1	$2 \times 10^{1} P_{N_2} \theta_*$	$N_2 + * \rightleftharpoons N_2*$	$2 \times 10^{14} e^{-43/(R_g T)} \theta_{N_2}$
2	$4 \times 10^{9} e^{-29/(R_g T)} \theta_{N_2} \theta_*$	$N_2* + * \rightleftharpoons 2N*$	$1 \times 10^{9} e^{-155/(R_g T)} (\theta_N)^2$
3	$2 \times 10^{9} e^{-81/(R_g T)} \theta_H \theta_N$	$H* + N* \rightleftharpoons NH* + *$	$1 \times 10^{7} e^{-23/(R_g T)} \theta_{NH} \theta_*$
4	$1 \times 10^{13} e^{-36/(R_g T)} \theta_{NH} \theta_H$	$NH* + H* \rightleftharpoons NH_2* + *$	$1 \times 10^{12} \theta_{NH_2} \theta_*$
5	$4 \times 10^{13} e^{-39/(R_g T)} \theta_{NH_2} \theta_H$	$NH_2* + H* \rightleftharpoons NH_3* + *$	$2 \times 10^{13} \theta_{NH_3} \theta_*$
6	$4 \times 10^{12} e^{-39/(R_g T)} \theta_{NH_3}$	$NH_3* \rightleftharpoons NH_3 + *$	$2 \times 10^{3} P_{NH_3} \theta_*$
7	$7 \times 10^{1} P_{H_2} (\theta_*)^2$	$H_2 + 2* \rightleftharpoons 2H*$	$3 \times 10^{13} e^{-94/(R_g T)} (\theta_H)^2$

[a] Rates are in units of molecules per second per site, pressures (P) are in pascals, and activation energies are in kilojoules per mole. Concentrations of surface species are represented by fractional surface coverages as discussed in Chapter 5. Kinetic parameters are adapted from the data of Stolze and Norskov [P. Stolze and J. K. Norskov, *Phys. Rev. Lett.*, **55** (1985) 2502; P. Stolze and J. K. Norskov, *Surf. Sci. Lett.*, **197** (1988) L230; P. Stolze and J. K. Norskov, *J. Catal.*, **110** (1988) 1].

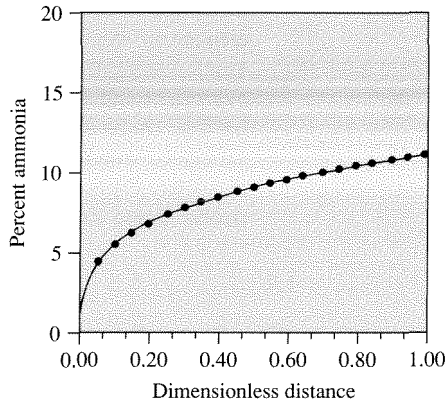

Figure 7.3.1 | Ammonia concentration calculated from microkinetic model versus longitudinal distance from reactor inlet. (Figure adapted from "Kinetic Simulation of Ammonia Synthesis Catalysis" by J. A. Dumesic and A. A. Trevino, in *Journal of Catalysis*, Volume 116:119, copyright © 1989 by Academic Press, reproduced by permission of the publisher and the authors.)

dinitrogen and dihydrogen. The space velocity was 16,000 h^{-1}, the catalyst bed density was 2.5 g cm^{-3}, and the catalyst site density was 6×10^{-5} mol g^{-1}. The ammonia concentration in the effluent of the reactor operating at 723 K was measured experimentally to be 13.2 percent. Figure 7.3.1 illustrates the ammonia concentration calculated from the microkinetic model as a function of axial distance along

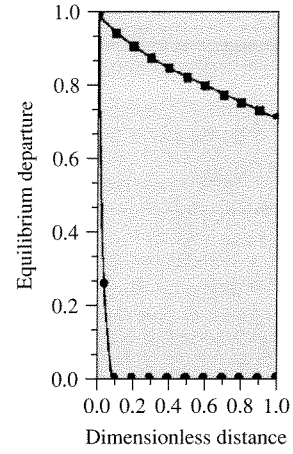

Figure 7.3.2 |
Departure from equilibrium for the two slowest elementary steps in ammonia synthesis. Squares are for step 2 and circles are for step 3. (Figure adapted from "Kinetic Simulation of Ammonia Synthesis Catalysis" by J. A. Dumesic and A. A. Trevino, in *Journal of Catalysis*, Volume 116:119, copyright © 1989 by Academic Press, reproduced by permission of the publisher and the authors.)

the reactor. The effluent concentration approached the experimental value of 13.2 percent, which illustrates the consistency of the model with observation. The utility of a microkinetic model, however, is that it allows for a detailed understanding of the reaction kinetics. For example, a rate-determining step can be found, if one exists, by examining the departure of the elementary steps from equilibrium under simulated reaction conditions. Figure 7.3.2 presents the departure from equilibrium, (forward rate − reverse rate)/forward rate, for the slowest steps as the reaction proceeds through the reactor. Step 2, the dissociation of dinitrogen, is clearly the rate-determining step in the mechanism throughout the reactor. All of the other steps in Table 7.3.1 are kinetically insignificant. Thus, the turnover frequency of ammonia synthesis depends critically on the kinetics of dissociative adsorption of dinitrogen (steps 1 and 2), as discussed earlier in Section 5.3. As long as the individual quasi-equilibrated elementary steps can be summed to one overall quasi-equilibrated reaction with a thermodynamically consistent equilibrium constant, small errors in the individual pre-exponential factors and activation energies are irrelevant. A microkinetic model also allows for the determination of relative coverages of various intermediates on the catalyst surface. Figure 7.3.3 illustrates the change in fractional surface reaction of N* and H* through the reactor. Adsorbed nitrogen is the most abundant reaction intermediate throughout the iron catalyst bed except at the entrance.

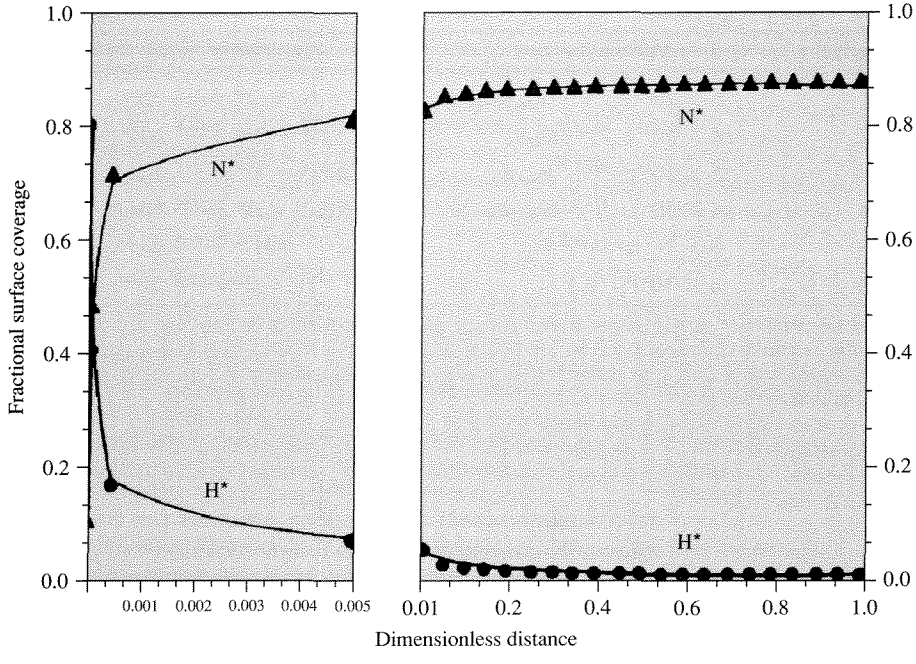

Figure 7.3.3 |
Fractional surface coverages of predominant adsorbed species versus dimensionless distance from the reactor inlet. (Figure adapted from "Kinetic Simulation of Ammonia Synthesis Catalysis" by J. A. Dumesic and A. A. Trevino, in *Journal of Catalysis*, Volume 116:119, copyright © 1989 by Academic Press, reproduced by permission of the publisher and the authors.)

Since the formation of N* is the rate-determining step, its high coverage during steady-state reaction on iron results from the equilibrium of H_2 and NH_3. Thus, the high coverage of H* instead of N* at the entrance to the reactor (Figure 7.3.3) results from the vanishingly low pressure of ammonia at that point.

Another test of validity is to check the performance of the model against experimental rate data obtained far from equilibrium. The microkinetic model presented in Table 7.3.1 predicts within a factor of 5 the turnover frequency of ammonia synthesis on magnesia-supported iron particles at 678 K and an ammonia concentration equal to 20 percent of the equilibrium value. This level of agreement is reasonable considering that the catalyst did not contain promoters and that the site density may have been overestimated. The model in Table 7.3.1 also predicts within a factor of 5 the rate of ammonia synthesis over an Fe(111) single crystal at 20 bar and 748 K at ammonia concentrations less than 1.5 percent of the equilibrium value.

It should be emphasized that since the rate of ammonia synthesis on iron depends critically on the dissociative adsorption of dinitrogen (steps 1 and 2), any

Table 7.3.2 | A proposed mechanism of ammonia synthesis over ruthenium catalysts.[a]

Number	Forward rate	Elementary step	Reverse rate
1	$6 \times 10^{-2} e^{-33/(R_g T)} P_{N_2} (\theta_*)^2$	$N_2 + 2* \rightleftharpoons 2N*$	$2 \times 10^{10} e^{-137/(R_g T)} (\theta_N)^2$
2	$6 \times 10^{13} e^{-86/(R_g T)} \theta_H \theta_N$	$H* + N* \rightleftharpoons NH* + *$	$3 \times 10^{14} e^{-41/(R_g T)} \theta_{NH} \theta_*$
3	$5 \times 10^{13} e^{-60/(R_g T)} \theta_{NH} \theta_H$	$NH* + H* \rightleftharpoons NH_2* + *$	$2 \times 10^{13} e^{-9/(R_g T)} \theta_{NH_2} \theta_*$
4	$3 \times 10^{13} e^{-17/(R_g T)} \theta_{NH_2} \theta_H$	$NH_2* + H* \rightleftharpoons NH_3* + *$	$9 \times 10^{12} e^{-65/(R_g T)} \theta_{NH_3} \theta_*$
5	$6 \times 10^{13} e^{-84/(R_g T)} \theta_{NH_3}$	$NH_3* \rightleftharpoons NH_3 + *$	$2 \times 10^3 P_{NH_3} \theta_*$
6	$6 \times 10^2 P_{H_2} (\theta_*)^2$	$H_2 + 2* \rightleftharpoons 2H*$	$2 \times 10^{13} e^{-89/(R_g T)} (\theta_H)^2$

[a] Rates are in units of molecules per second per site, pressures (P) are in pascals, and activation energies are in kilojoules per mole. Concentrations of surface species are represented by fractional surface coverages as discussed in Chapter 5. Kinetics parameters are adapted from the data of Hinrichsen et al. [O. Hinrichsen, F. Rosowski, M. Muhler, and G. Ertl, *Chem. Eng. Sci.*, **51** (1996) 1683.]

microkinetic model that properly accounts for those steps and that is thermodynamically consistent with the overall reaction will effectively describe the kinetics of ammonia synthesis. This feature explains the success of the microkinetic model used to describe an industrial reactor even though the kinetic parameters for dinitrogen adsorption/desorption match those obtained from studies on iron single crystals in ultrahigh vacuum.

Ammonia synthesis on supported ruthenium catalysts has also been the subject of microkinetic analysis. Table 7.3.2 presents the kinetic parameters for one model of ammonia synthesis catalyzed by cesium-promoted ruthenium particles supported on MgO [O. Hinrichsen, F. Rosowski, M. Muhler, and G. Ertl, *Chem. Eng. Sci.*, **51** (1996) 1683]. In contrast to the model in Table 7.3.1, the dissociative adsorption of dinitrogen is represented by a single step. Many of the rate constants in Table 7.3.2 were determined from independent steady-state and transient experiments on the same catalyst. The experiments included temperature-programmed adsorption and desorption of dinitrogen, isotopic exchange of labeled and unlabeled dinitrogen, and temperature-programmed reaction of adsorbed nitrogen atoms with gaseous dihydrogen. The unknown rate constants were estimated by regression analysis of the experimental data and checked to ensure that they were within physically reasonable limits. As in the previous example with the iron catalyst, the steady-state reactor containing the supported Ru catalyst was modeled as a series of mixing cells in which the steady-state rate equations, the catalyst site balance and the material balances for gaseous species were solved simultaneously.

Similar to the results found with iron catalysts, the rate-determining step during ammonia synthesis on ruthenium catalysts is the dissociative adsorption of dinitrogen. However, the overall reaction rate is strongly inhibited by dihydrogen, indicating that adsorbed hydrogen is the most abundant reaction intermediate that covers most of the surface [B. C. McClaine, T. Becue, C. Lock, and R. J. Davis,

J. Mol. Catal. A: Chem., **163** (2000) 105]. In the example using iron catalysts, inhibition by dihydrogen was observed only at extremely low pressures of ammonia. The reaction on ruthenium is quite different, since the equilibrium involving dihydrogen and ammonia on the catalyst surface continues to favor hydrogen atoms instead of nitrogen atoms, even at reasonable pressures of ammonia. The microkinetic model in Table 7.3.2 accounts for the ammonia effluent concentration from a reactor operating at both atmospheric pressure and elevated pressure, over a wide temperature range and at exit conditions near and far from equilibrium. Figure 7.3.4 compares

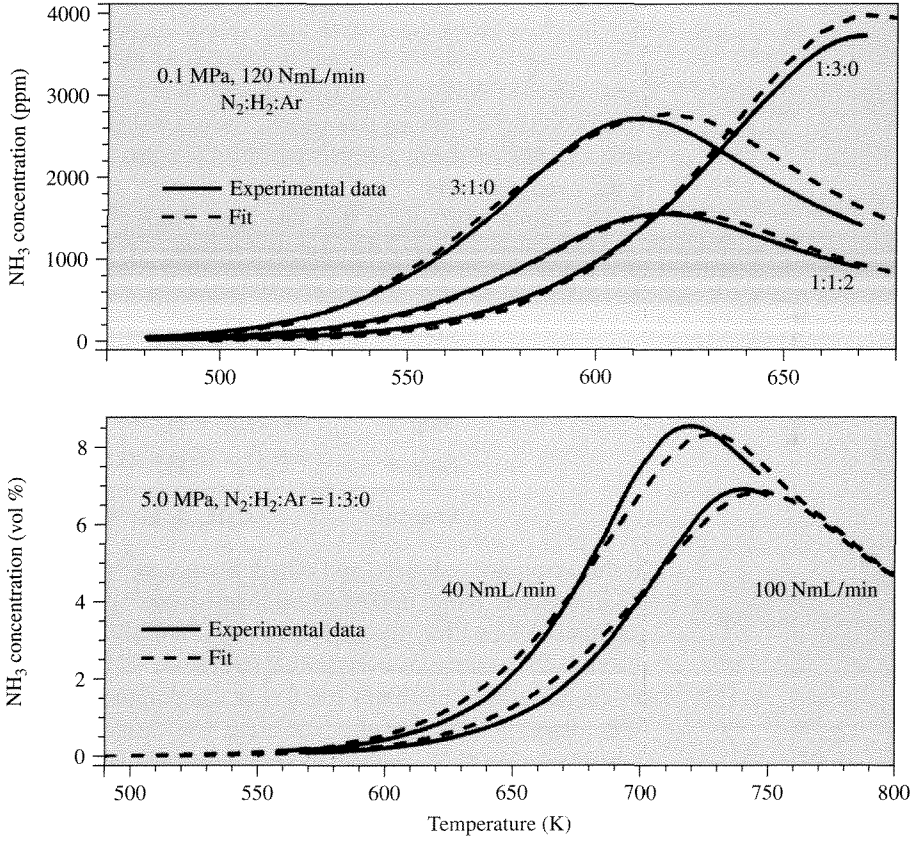

Figure 7.3.4 |
Comparison of calculated and measured ammonia concentrations at the effluent of a steady-steady ammonia synthesis reactor containing ruthenium particles supported on magnesia and promoted by cesium. [Adapted from O. Hinrichsen, F. Rosowski, M. Muhler, and G. Ertl, "The Microkinetics of Ammonia Synthesis Catalyzed by Cesium-Promoted Supported Ruthenium," *Chem. Eng. Sci.*, **51** (1996) 1683, copyright 1996, with permission from Elsevier Science.]

the results from the model to those measured experimentally. The decrease in ammonia effluent concentration at the highest temperatures indicates that equilibrium was reached in the reactor. The essential features of the reaction (i.e., proper temperature dependence of the rate appropriate level of ammonia produced near and far from equilibrium, and inhibition of the rate by dihydrogen) were well reproduced by the kinetic model.

7.4 | Ethylene Hydrogenation on Transition Metals

Hydrogenation is an important industrial reaction that often requires the presence of a heterogeneous catalyst to achieve commercial yields. Ethylene, C_2H_4, is the smallest olefin that can be used to investigate the addition of hydrogen atoms to a carbon-carbon double bond. Even though many experiments and theoretical studies have been carried out on this simple system, the reaction is still not completely understood. Microkinetic analysis provides insights into the relevant elementary steps in the catalytic cycle.

A simple mechanism that has been proposed for ethylene hydrogenation on metal catalysts is that of Horiuti and Polanyi [J. Horiuti and M. Polanyi, *J. Chem. Soc., Faraday Trans.*, **30** (1934) 1164]:

Step 1	$H_2 + 2^* \rightleftharpoons 2H^*$
Step 2	$C_2H_4 + 2^* \rightleftharpoons {}^*C_2H_4{}^*$
Step 3	${}^*C_2H_4{}^* + H^* \rightleftharpoons {}^*C_2H_5 + 2^*$
Step 4	${}^*C_2H_5{}^* + H^* \rightleftharpoons {}^*C_2H_6 + 2^*$
Overall	$C_2H_4 + H_2 = C_2H_6$

In this sequence, ethylene and dihydrogen compete for active sites on the transition metal surface. While this basic mechanism has been used to describe olefin hydrogenation kinetics for many years, it does not adequately account for the observed reaction characteristics over a wide range of conditions. For example, ethylene hydrogenation on a platinum catalyst at temperatures less than 300 K is zero-order with respect to ethylene and half-order with respect to dihydrogen. The zero-order dependence on C_2H_4 indicates that the surface is nearly covered with carbon containing species, whereas the half-order dependence on H_2 suggests that step 1, dissociative adsorption of dihydrogen, is an equilibrated process. If the adsorption steps were truly competitive, then increasing the ethylene pressure should decrease the vacant site concentration and thus the hydrogen surface coverage. In other words, the rate of hydrogenation should decrease with increasing ethylene pressure, which is not observed at low temperature.

One way to explain the observed reaction orders is to also allow for a *noncompetitive* dihydrogen adsorption step in the sequence. This added complexity makes sense because more surface sites are available to dihydrogen than ethylene because of the very small size of a H_2 molecule. The catalytic cycle for ethylene

hydrogenation with both *competitive* and *noncompetitive* adsorption is now:

Step 1	$H_2 + 2* \rightleftharpoons 2H*$
Step 1a	$H_2 + 2*' \rightleftharpoons 2H*'$
Step 2	$C_2H_4 + 2* \rightleftharpoons *C_2H_4*$
Step 3	$*C_2H_4* + H* \rightleftharpoons *C_2H_5 + 2*$
Step 3a	$*C_2H_4* + H*' \rightleftharpoons *C_2H_5 + * + *'$
Step 4	$*C_2H_5 + H* \rightleftharpoons C_2H_6 + 2*$
Step 4a	$*C_2H_5 + H*' \rightleftharpoons C_2H_6 + * + *'$
Overall	$C_2H_4 + H_2 = C_2H_6$

where *′ represents an active site that is accessible to dihydrogen but not to ethylene. Rekoske et al. have studied an analogous sequence of steps for ethylene hydrogenation on Pt, but their analysis also included a hydrogen activation step [J. E. Rekoske, R. D. Cortright, S. A. Goddard, S. B. Sharma, and J. A. Dumesic, *J. Phys. Chem.*, **96** (1992) 1880]. The additional activation step was needed to reconcile results from microkinetic analysis to the observed isotopic distribution of products when deuterium was added to the system. Nevertheless, their analysis showed that the main features of Pt-catalyzed ethylene hydrogenation could be captured over a very wide range of conditions by the coupled competitive and noncompetitive mechanism of Horiuti and Polanyi. Figure 7.4.1 compares the measured and calculated turnover frequencies over an order of magnitude range

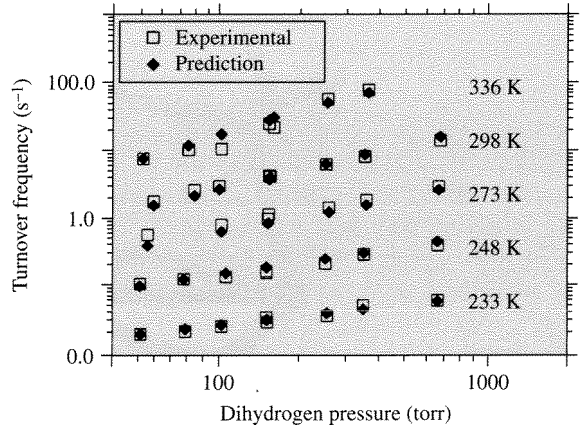

Figure 7.4.1 |
Comparison of results from microkinetic model and experimental observation. [Adapted with permision from J. E. Rekoske, R. D. Cortright, S. A. Goddard, S. B. Sharma, and J. A. Dumesic, *J. Phys. Chem.*, **96** (1992) 1880. Copyright 1992 American Chemical Society.]

of dihydrogen pressure and a 100 K span in temperature. The observed order of reaction with respect to dihydrogen increases from 0.47 at 223 K to 1.10 at 336 K. Clearly, the kinetic model reproduces the observed rates at all of the conditions tested. The model also predicted the order of reaction with respect to ethylene (not shown) quite well. This microkinetic analysis suggests that ethylene hydrogenates mostly through the noncompetitive route at low temperatures whereas the competitive route dominates at high temperatures.

The rapid increase in computing power and the advent of new quantum chemical methods over the last decade allow kinetic parameters for surface reactions to be estimated from *ab initio* quantum chemical calculations and kinetic simulation schemes. Indeed, the adsorption enthalpies of gas-phase species can be calculated, the activation barriers to form transition states from surface bound species can be predicted, and the evolution of surface species with time can be simulated. Figure 7.4.2 shows, for example, the transition state for the hydrogenation of adsorbed ethylene (step 3) on a model palladium surface consisting of 7 Pd atoms arranged in a plane. The activation energy associated with ethyl formation on a Pd(111) metal surface was calculated from first principles quantum mechanics to be about 72 kJ mol^{-1} [M. Neurock and R. A. van Santen, *J. Phys. Chem. B,* **104** (2000) 11127]. The configuration of the adsorbed ethyl species, the product of step 3, is illustrated for two different Pd surfaces in Figure 7.4.3. The energies for chemisorption of this reactive intermediate on a Pd_{19} cluster and a semi-infinite Pd(111) slab are –130 and –140 kJ mol^{-1}, respectively, and are essentially the same within the error of the calculation. Results involving adsorbed ethylene, adsorbed hydrogen and adsorbed ethyl indicate

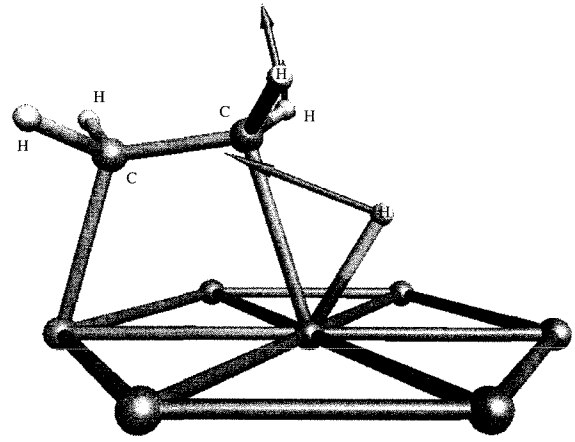

Figure 7.4.2 |
The isolated transition state structure for the formation of ethyl from ethylene and hydrogen on a model Pd_7 cluster. The vectors correspond to the motion along the reaction coordinate. [Adapted with permission from M. Neurock and R. A. van Santen, *J. Phys. Chem. B,* **104** (2000) 11127. Copyright 2000 American Chemical Society.]

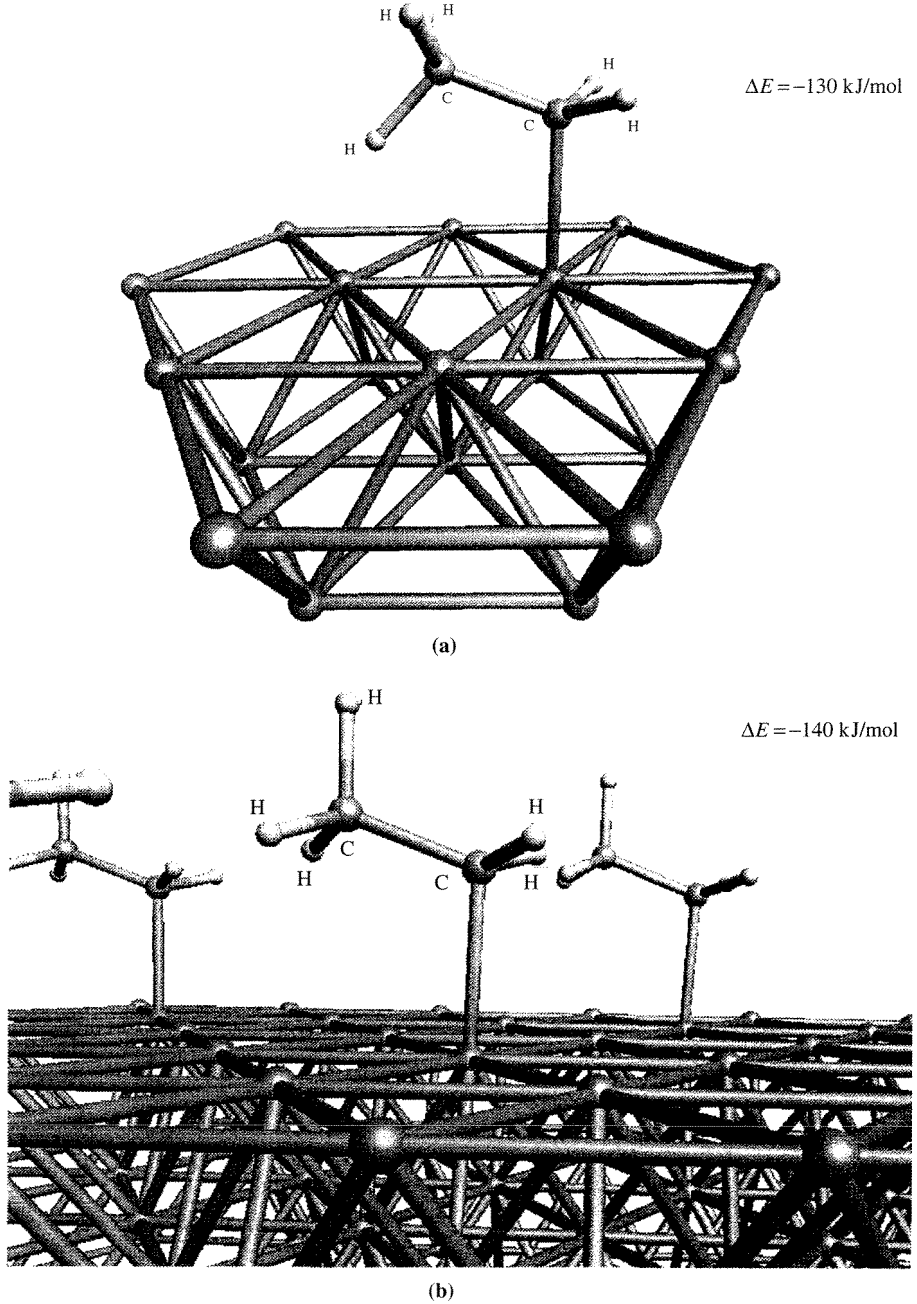

Figure 7.4.3 |
Structures and energies for the chemisorption of ethyl on (**a**) a Pd_{19} cluster model and (**b**) a model Pd(111) surface. [Reproduced with permission from M. Neurock and R. A. van Santen, *J. Phys. Chem. B*, **104** (2000) 11127. Copyright 1992 American Chemical Society.]

that the overall heat of reaction for step 3 is about 3 kJ mol^{-1} endothermic on a Pd surface. In principle, these types of calculations can be performed on all of the species in the Horiuti-Polanyi mechanism, and the results can be used in a subsequent kinetic simulation to ultimately give a reaction rate. Rates obtained in this fashion are truly from first principles since regression of experimental data is not required to obtain kinetic parameters.

Hansen and Neurock have simulated the hydrogenation of ethylene on a Pd catalyst using a Monte Carlo algorithm to step through the many reactions that occur on a model surface [E. W. Hansen and M. Neurock, *J. Catal.*, **196** (2000) 241]. In essence, the reaction is simulated by initializing a grid of Pd atoms and allowing all possible reactions, like adsorption of reactants, elementary surface reactions, and desorption of products, to take place. The simulation moves forward in time, event by event, updating the surface composition as the reaction proceeds. The details of the method are too complicated to describe here but can be found in E. W. Hansen and M. Neurock, *J. Catal.*, **196** (2000) 241. The input to the simulation involves a complete set of adsorption and reaction energies. An important feature of this simulation is that it also accounts for interactions among the species on the surface.

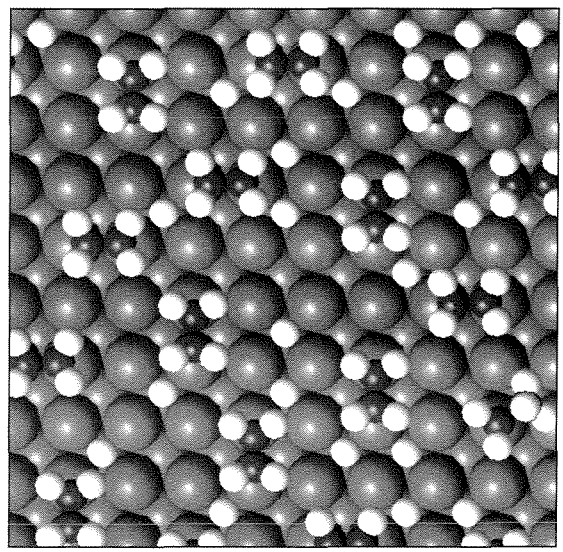

Figure 7.4.4 |
Snapshot of a Pd(100) surface during a simulation of ethylene hydrogenation at 298 K, 25 torr of ethylene and 100 torr of dihydrogen. [Figure from "First-Principles-Based Monte Carlo Simulation of Ethylene Hydrogenation Kinetics on Pd," by E. W. Hansen and M. Neurock, in *Journal of Catalysis*, Volume 196:241, copyright © 2000 by Academic Press, reproduced by permission of the publisher and authors.]

Although many kinetic models assume that the catalyst is an ideal Langmuir surface (all sites have identical thermodynamic properties and there are no interactions among surface species), modern surface science has proven that ideality is often not the case.

Results from the simulation reproduced the experimentally observed kinetics (activation energy, turnover frequency, and orders of reaction) for ethylene hydrogenation on a Pd catalyst. A snapshot of the Pd surface during a simulation of ethylene hydrogenation is given in Figure 7.4.4. At this point in the simulation, highly mobile hydrogen atoms moved rapidly around the surface and reacted with fairly stationary hydrocarbons. In this model, no distinction was made between the competitive and noncompetitive adsorption steps in the mechanism. The results suggest that lateral interactions among species can explain some of the experimental observations not easily accounted for in the Horiuti-Polanyi mechanism.

7.5 | Concluding Remarks

This chapter illustrated the concepts involved in microkinetic analysis of catalytic reactions. The first example involving asymmetric hydrogenation of prochiral olefins with a chiral homogeneous catalyst illustrated how precise rate measurements of critical elementary steps in a catalytic cycle can yield a kinetic model that describes the overall performance of a reaction in terms of enantioselectivity and response to reaction conditions. The second example regarding ammonia synthesis showed how kinetic parameters of elementary steps measured on single crystals under ultrahigh vacuum conditions can be incorporated into a kinetic model that applies to reactors operating under industrial conditions of high pressure. The last example involving ethylene hydrogenation revealed how quantum chemical calculations provide estimates of the energies associated with elementary steps on catalytic surfaces that can be subsequently used in reaction simulations. Finally, microkinetic analysis is clearly moving toward the routine use of quantum chemical calculations as inputs to kinetic models, with the ultimate goal of describing industrial chemical reactors.

Exercises for Chapter 7

1. In Section 7.2, the reaction paths of the Rh-catalyzed asymmetric hydrogenation of **MAC** were described in detail. The ratio of the **S** product to the **R** product, [**S**]/[**R**], was expressed in the limit of low [Equation (7.2.16)] and high [Equation (7.2.22)] pressure (or concentration) of dihydrogen. Use the rate constants in Table 7.2.1 to plot [**S**]/[**R**] as a function of H_2 concentration. At what concentrations are Equation (7.2.16) and Equation (7.2.22) valid?
2. Landis and Halpern studied the temperature dependence of the various rate constants in Table 7.2.1 [C. R. Landis and J. Halpern, *J. Am. Chem. Soc.*, **109** (1987) 1746]. The values of the individual activation energies and preexponential factors are:

Kinetic parameters for the asymmetric hydrogenation of MAC catalyzed by Rh(R,R-DIPAMP).

Parameter	R cycle		S cycle	
	E^a	$\bar{A}^b$	E^a	$\bar{A}^b$
k_1 (L mmol^{-1} s^{-1})	4.9	2.32×10^4	6.9	1.21×10^6
k_{-1} (s^{-1})	13.3	8.53×10^8	13.0	9.94×10^9
k_2 (L mmol^{-1} s^{-1})	10.7	7.04×10^4	7.5	1.84×10^5

[a] Activation energy, kcal mol^{-1}.
[b] Pre-exponential factor in the units of the rate constant.
Source: C. R. Landis and J. Halpern, *J. Am. Chem. Soc.*, **109** (1987) 1746.

Determine the ratio of the **S** product to the **R** product, [**S**]/[**R**], as a function of temperature, over the range of 0 to 37°C. Keep the H_2 concentration at a constant value between the limits of high and low pressure as discussed in Exercise 1.

3. A microkinetic analysis of ammonia synthesis over transition metals is presented in Section 7.3. Use the results of that analysis to explain how adsorbed nitrogen atoms (N*) can be the most abundant reaction intermediate on iron catalysts even though dissociative chemisorption of N_2 is considered the rate-determining step.

4. Describe the main differences in the kinetics of ammonia synthesis over iron catalysts compared to ruthenium catalysts.

5. The Horiuti-Polanyi mechanism for olefin hydrogenation as discussed in Section 7.4 involves 4 steps:

Step 1	$H_2 + 2^* \rightleftarrows 2H^*$
Step 2	$C_2H_4 + 2^* \rightleftarrows {}^*C_2H_4{}^*$
Step 3	${}^*C_2H_4{}^* + H^* \rightleftarrows {}^*C_2H_5 + 2^*$
Step 4	${}^*C_2H_5 + H^* \rightleftarrows C_2H_6 + 2^*$
Overall	$C_2H_4 + H_2 = C_2H_6$

Derive a rate expression for the hydrogenation of ethylene on Pt assuming steps 1, 2, and 3 are quasi-equilibrated, step 4 is virtually irreversible, and ${}^*C_2H_5$ is the most abundant reaction intermediate covering almost the entire surface ($[^*]_0 \sim [{}^*C_2H_5]$). Discuss why the rate expression cannot properly account for the experimentally observed half order dependence in H_2 and zero-order dependence in ethylene. Could the observed reaction orders be explained if adsorbed ethylene (${}^*C_2H_4{}^*$) were the most abundant reaction intermediate? Explain your answer.

6. Read the paper entitled "Microkinetics Modeling of the Hydroisomerization of n-Hexane," by A. van de Runstraat, J. van Grondelle, and R. A. van Santen, *Ind. Eng. Chem. Res.*, **36** (1997) 3116. The isomerization of n-hexane is a classic

example of a reaction involving a bifunctional catalyst, where a transition metal component facilitates hydrogenation/dehydrogenation and an acidic component catalyzes structural rearrangement. Section 5.3 illustrates the important reactions involved in hydrocarbon isomerization over bifunctional catalysts. Summarize the key findings of the microkinetic analysis by van de Runstraat et al.